Fuel 371 (2024) 132136

Contents lists available at ScienceDirect

Fuel

journal homepage: www.elsevier.com/locate/fuel

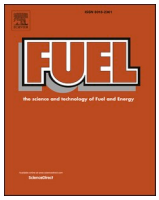

Full Length Article

An investigation of monolithic nickel-based catalyst for clean hydrogen production with CCS technology: The effect of structure

Ziqi Shen *, Seyed A. Nabavi, Peter T. Clough

Energy and Sustainability Theme, Cranfield University, Cranfield, Bedfordshire MK43 0AL, UK

ARTICLE INFO

Keywords:
Structured catalysts
Structure
Steam methane reforming
Hydrogen production
Carbon capture

ABSTRACT

At present, hydrogen is recognised as a carbon-free energy carrier, but its major production via the steam methane reforming (SMR) process requires further decarbonisation as a considerable amount of carbon dioxide is simultaneously emitted. Carbon capture and storage (CCS) techniques can be integrated with typical SMR to produce clean hydrogen. Previously, a novel structured catalyst (Ni/SiC-M) was developed, and it was highly active for SMR under low operating temperature and high gas space velocity. By integrating CCS techniques, this structured catalyst is promising to produce clean hydrogen, however, there is a lack of knowledge about the catalytic performance when CCS is applied, especially the effect of structure. In this work, the feasibility of producing cleaner hydrogen with monolithic catalysts (Ni/SiC-M) coupled with sorbent particles was discussed. Different modified structures were applied for performance evaluation with a fixed bed reactor, to better understand the relationship between the structure and the activity. The results showed that sorbent particles can adsorb most of the generated carbon dioxide, leading to a higher hydrogen purity; the limitation of internal mass transfer caused by high pressure drops can result in a decrease in catalytic activity, but the impact was limited. The pore size could be the key factor to influence the performance of structured catalysts.

1. Introduction

Climate change is considered to be a great threat to our society. The use of fossil fuels during the last two centuries is the main cause of this crisis, as stated by the Intergovernmental Panel on Climate Change (IPCC) in 2007 [1,2]. The global temperature increase is likely to surpass the limit of 1.5 °C before other energy sources replace fossil fuels [3], and the first yearly breach was observed in July 2023, according to the global temperature trend monitor published on the EU's Copernicus Climate Change Service's website [4]. Hydrogen has drawn attention for decades as a clean energy carrier, although currently, most hydrogen is produced via steam methane reforming (SMR), which uses natural gas as the feedstock [5]. This process is usually represented by the steam reforming of methane reaction (Eq. (1)) and the water–gas shift reaction (Eq. (2)):

$$CH_4 + H_2O \leftrightarrow CO + 3H_2 \quad \Delta H^{\circ}_{298} = +206kJ \bullet mol^{-1} \tag{1}$$

$$CO + H_2O \leftrightarrow CO_2 + H_2 \quad \Delta H^{\circ}_{298} = -41kJ \bullet mol^{-1} \tag{2}$$

These reactions reveal the source of a high content of CO_2 during the SMR process, with a high emission factor of about 10 tCO_2/tH_2 [6]. The decarbonisation of SMR becomes the key feature here, and much attention has been paid to the carbon capture and storage (CCS) process [7]. Another perspective to produce clean hydrogen is the application of the photocatalysts with S-scheme heterojunction [8], such as the Co catalyst supported on $CuMn_2O_4$/graphdiyne composites [9]. With CCS techniques, the carbon capture rate can reach 90 % when syngas is treated [10]. Sorption-enhanced steam methane reforming (SE-SMR) could be one of the solutions for clean hydrogen production, where CCS technology (which could be *in-situ*) is coupled with SMR. Due to the low cost and high availability, CaO-based sorbents are recognised as promising candidates [11]. The following reversible reaction can represent the additional reaction that takes place in a typical SE-SMR process (Eq. (3)). CO_2 is absorbed by CaO-based sorbents via carbonation in a temperature range of 600–800 °C and the sorbents can be regenerated via calcination at a temperature above 800 °C [12]. It was also found that the diffusion of CO_2 was restricted when the temperature was higher than 515 °C as a compact $CaCO_3$ layer formed [13].

$$CO_2 + CaO \leftrightarrow CaCO_3 \quad \Delta H^{\circ}_{298} = -176kJ \bullet mol^{-1} \tag{3}$$

* Corresponding author.
E-mail address: ziqi.shen@cranfield.ac.uk (Z. Shen).

https://doi.org/10.1016/j.fuel.2024.132136
Received 31 March 2024; Received in revised form 20 May 2024; Accepted 4 June 2024
Available online 8 June 2024

Nickel-based catalysts in the SMR process were renowned for their cheaper price and relatively good reactivity [14]. The support plays an important role in the catalyst, and some materials can be added to enhance the activity (e.g. metal, oxides). For example, the catalytic activity of the Ni-Zn-Al catalyst was reported to be higher than the common Ni/α-Al_2O_3 and Ni/SiO_2 catalysts at low temperatures [15]. Obradović et al. developed a novel nickel plate catalyst with Pt and Al_2O_3 coating and demonstrated its good activities and kinetics at low temperatures (below 590 °C) [16,17]. The performance of nickel-based catalysts can be also enhanced by their structure. Lorber et al. compared the catalytic activity of nickel-based catalysts with three different shapes of ceria supports, nanorod, nanocube, and nanosphere, and the nanorod exhibited better metal dispersion to be more active than others [18]. Using silicon carbide (SiC), a highly-efficient monolithic catalyst (Ni/SiC-M) was developed [19]. As with other nickel-based catalysts, the product via SMR was a mixture of H_2, CO_2, CO, and unreacted CH_4, with a volumetric concentration of hydrogen of 72 % at 600 °C. The integration of CCS technology is a feasible way to filter the exhaust gas, as it can sequestrate the remaining CO_2 easily. However, the good activity of the structured catalyst was attributed to its structure, as the pores and channels of the structured catalysts can decrease internal mass transfer limitations under high space velocity and low pressure [20]. However, it is still unclear whether the catalysts are as active as under SMR conditions when sorbents are added. Therefore, it would be of interest to investigate the relationship between the porous structures and the catalytic activities of the material under SE-SMR conditions.

In this work, a typical calcium sorbent was applied over monolithic nickel-based catalysts, with different pore structures and properties. The pore size and shape of the monolithic supports were studied, as well as the sorbent particle size. A feasible design was selected and all experiments were conducted with a fixed-bed reactor under the same operating conditions (600 °C, 1 bar, space velocity 10,000 h^{-1}, steam to carbon ratio 3) to evaluate the catalytic performance of different samples. Carbon dioxide was adsorbed efficiently by the sorbents while the hydrogen purity increased to 80 %, although methane conversion was found to be lower. The reason for the lower methane conversion was the increased mass transfer limitation through the pores due to the increase of pressure drops, regardless of the shape of the pores. To achieve higher performance, attention should be focused on the trade-off between enlarging the pores and the potential range of sorbent particles for further improvement.

2. Experimental

2.1. Materials and catalyst/sorbent preparation

The modified freeze-gelation method (standard protocol) described in our previous work was used for the monolithic support synthesis [19]. It was recognised as a sacrificial template method to produce SiC ceramics, and the pore former was water (ice) [21]. The structure of the monolithic catalyst prepared with the standard protocol was assumed to be identical, as the pore former was assumed to have the same characteristics when the processing conditions (e.g. temperatures, durations, pressures, etc) are kept the same. However, in order to restructure the monolith, Fukushima et al. indicated that the freezing temperature significantly impacted the pore structure. When the freezing temperature decreased (from −10 to −70 °C), they found that the average pore size was reduced, and the number of pores was increased, as the size of the ice crystals (pore formers) was smaller at lower temperatures [22]. Another way is to apply another agent (s). As summarised by Hotza et al., other pore formers (e.g. polymethyl methacrylate) can function in a similar way to build different porous structures [23]. The structure of the catalyst may also be stabilised by appropriate additives [24]. In this study, polymethyl methacrylate (PMMA, molar weight 15,000, GPC) purchased from Sigma Aldrich was selected as the second additive to affect the structural properties of catalysts. For the sorbent, various grades of limestone granules (Longcliffe LONGCAL) which have a minimum 98.25 % content of calcium carbonate were used.

Table 1
Compositions and freezing conditions of samples in this study.

Samples	Compositions	Freezing conditions
SiC-M and SiC-M-old	SiC:Al_2O_3:ZrO_2 = 96:2.4:1.6; Gelatine: 10 wt%	Freezing at −18.5 °C
SiC-M-40C and SiC-M-40C-old	SiC:Al_2O_3:ZrO_2 = 96:2.4:1.6; Gelatine: 10 wt%	Freezing at −40 °C
SiC-M-70C	SiC:Al_2O_3:ZrO_2 = 96:2.4:1.6; Gelatine: 10 wt%	Freezing at −70 °C
SiC-M-10PMMA	SiC:Al_2O_3:ZrO_2 = 96:2.4:1.6; Gelatine: 10 wt%; PMMA: 10 wt%	Freezing at −18.5 °C
SiC-M-20PMMA and SiC-M-20PMMA-old	SiC:Al_2O_3:ZrO_2 = 96:2.4:1.6; Gelatine: 10 wt%; PMMA: 20 wt%	Freezing at −18.5 °C

In this work, two methods (reducing freezing temperatures and adding other agents) were employed to modify the structure of monolithic catalysts. Only one condition was changed each time, to establish the modified protocols of the catalyst support preparation. For the first method, two different freezing temperatures (−40 and −70 °C) were chosen to achieve significant temperature gradients. For the second method, PMMA powder was weighed before mixing with the 10 wt% gelatine solution. The pre-mixed dry powder that contained silicon carbide (SiC) and sintering aids (aluminium oxide and zirconia oxide) was then slowly poured into the suspending solution when no apparent plastic paste could be identified, as PMMA were considered to be insoluble in water at about 35 °C. The new slurries were frozen at −18.5 °C overnight before further treatments. These samples were treated afterward using the same protocol described in our previous study [19]. The green body of the monolithic supports was made after water and organic compounds were removed by freeze-drying and calcination (at 600 °C). The structure of the green body was then intensified by thermal sintering (at 1400–1500 °C). The monoliths were formed into a cylindrical shape with a similar size of SiC-M, whose dimensions were 20.2 ± 0.18 mm in diameter and 16.8 ± 0.20 mm in height [19]. Table 1 summarises the detailed compositions and freezing conditions of different monoliths in this study:

To avoid errors from the nickel loading process, the wet impregnation technique was applied, under the same conditions used in our previous study [19]. It is assumed that there is no significant change in the performance of NiO crystallite deposition using SiC-M monoliths and other samples, as the surfaces of these catalyst supports were the same. Herein, only one concentration of the precursor solution was chosen, which contained 20 wt% of nickel(II) nitrate hexahydrate ($Ni(NO_3)_2{\cdot}6H_2O$, 99 %, Thermo Scientific), by mixing 15.91 g of nickel salts with 44.09 g of deionised water. Air was removed before immersion of monoliths and the operating conditions of impregnation and calcination were precisely controlled, as shown for 20Ni/SiC-M catalyst preparation in our previous work [19]. The samples were denoted as 20Ni/SiC-M-x, in which *x* represents the modification of samples listed in Table 1 (e.g. 20Ni/SiC-M-40C).

Three grades of limestone granules were selected as the sorbent: small (200–315 μm), middle (315–400 μm), and big (400–500 μm). All limestones were pretreated using multiple stainless steel sampling sieves (Titan) with appropriate ranges and were kept at 80 °C to avoid high moisture contamination until the fresh catalysts had been prepared.

2.2. Catalyst characterisation

To evaluate the actual nickel loading of various SiC-M supports, all monoliths were assumed to be rigid before and after the complete calcination of impregnated samples, and the mass balance of nickel (nickel nitrates and nickel oxides) was established for nickel nitrates

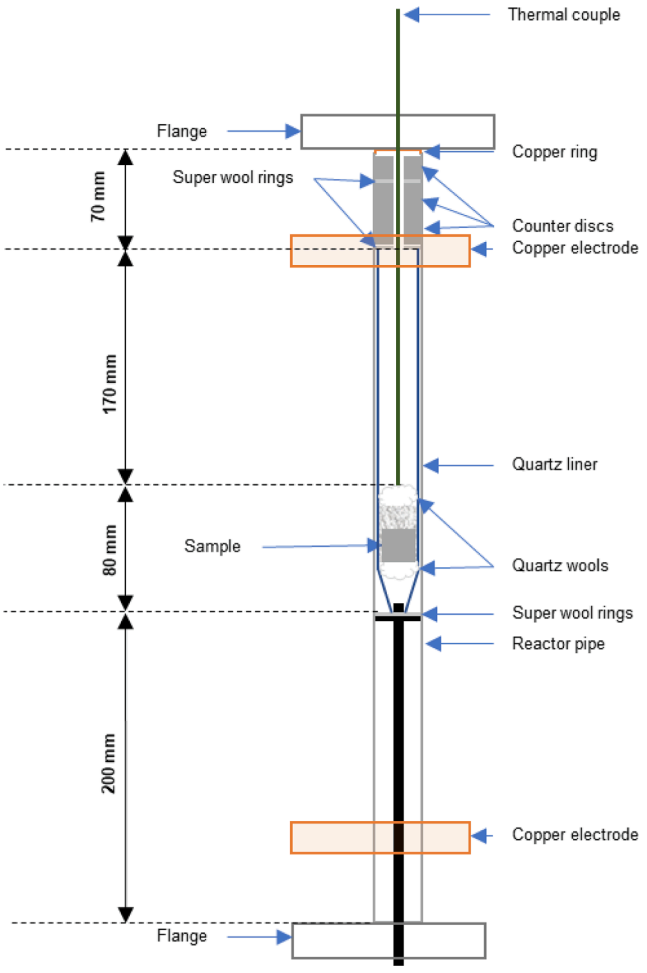

Fig. 1. Reaction configuration used in this study.

decomposition. The structural properties of various SiC-M supports were measured using mercury intrusion porosimetry (MIP). The samples include 'old batch' samples that were previously sintered in air at 1500 °C (denoted as 'SiC-M-old', 'SiC-M-40C-old' and 'SiC-M-20PMMA-old') and a 'new batch' sample for comparison (denoted as 'SiC-M'), which was sintered in 100 mL•min^{-1} pure nitrogen flow at 1400 °C. A micrometric AutoPore IV 9500 analyser was used to evaluate the characteristics of pores (e.g. porosity). A 3P Meso 222 model physisorption analyser was used to obtain nitrogen adsorption isotherms at 77 K for the samples (old and new batches), and Brunauer, Emmett, and Teller (BET) specific surface area was evaluated. The morphology of different SiC-M catalyst supports (including old and new batches) was investigated via scanning electron microscopy (SEM) using a Tescan Vega 3 instrument at 20 kV.

2.3. Catalytic performance test

All tests were performed under one single operating condition (600 °C, 1 bar, steam to carbon ratio of 3, gas hourly space velocity (GHSV) of 10,000 h^{-1}), which was the optimal SMR operating condition using 20Ni/SiC-M in our previous study [19]. The primary tests were carried out with the original monolithic catalysts 20Ni/SiC-M and the middle grade of limestone. These tests aimed to demonstrate the feasibility of the designs, where the sorbent granules were physically mixed with the monolithic catalysts. As the sorbent was supposed to adsorb carbon dioxide produced via the SMR process (Eq. (1) and (2)) as much as possible, an excessive amount of sorbent in the system was required. The amount of sorbent used for each test was calculated based on the test duration for each sample. Herein, about 1.8 g of catalyst and 3.0 g of activated sorbent granules were applied, and the tests were performed for 10–15 mins as the reaction reached its steady state within this short duration. Once the optimal design was selected, sorbents in different particle size ranges were tested, coupled with the standard monolithic 20Ni/SiC-M catalysts. Furthermore, the original 20Ni/SiC-M catalysts in the selected design were replaced with one of the other structured catalysts (20Ni/SiC-M-40C, 20Ni/SiC-M-70C, 20Ni/SiC-M-10PMMA, or 20Ni/SiC-M-20PMMA), while the same range of particle size was maintained for the sorbents. The sorbents were activated by calcination in air at 900 °C for 2 h in a muffle furnace and were immediately used for the tests once the calcination was completed. Sorbent deactivation by carbon dioxide was considered to be negligible as carbonation can be neglected at ambient conditions [25,26].

The experiments for the evaluation of SE-SMR catalytic activity and performance were conducted using a fixed-bed reactor that was described in our previous work [19]. The configuration of the reaction system was slightly adjusted, compared with the one for SMR performance testing. The K-type thermocouple monitoring the bed temperature was raised for a distance of 20 mm to achieve better contact with the upper surface of the sorbent layer (shown in Fig. 1). The catalysts and sorbents were packed between two layers of quartz wool to keep their position and were placed in the middle of the quartz liner.

This fixed-bed reactor system allows a maximum of three different gases to be sent, including N_2, 10 vol% CH_4 in N_2, and 10 vol% H_2 in N_2 mixtures, through three independent mass flow controllers (Bronkhorst UK). All gases were purchased from BOC. No further dilution was carried out during the experiments. The steam, which was generated through the steam generator by sending deionised water with a high-performance liquid chromatography (HPLC) pump (Jasco, model PU1586), was introduced with a flow of carrier gas (N_2) when needed.

Unlike the activation of sorbents, the activation of the catalysts took place inside the reactor. A continuous flow (20 mL/s) of 10 vol% hydrogen/nitrogen gas mixture was fed to the reactor and the operating temperature was maintained at 600 °C. After 10 mins, when no further steam generation was observed and hydrogen concentration reached the initial level, the catalysts were completely activated. After the whole system was reinitialised with N_2 flow, steam was introduced, followed by the gas mixture of methane/nitrogen when the flow rate of steam was stable. The steam generation and consumption rates were monitored by a Vaisala HMT330 series humidity probe. The outlet temperature of the exhaust gas was kept at over 100 °C. A continuous multi-gas analyser (NOVA 976PS model) was used to measure the gas concentrations of CH_4, H_2, CO, and CO_2 (in vol.%) at one-second intervals, with a response time of ~1.7 s. As the gas analyser required an anhydrous gas flow, moisture was removed through a water-cooled condenser, coupled with a $CaCl_2$ water trap, before the sample gas was sent to the gas analyser.

Methane conversion, hydrogen yield, hydrogen purity, and carbon monoxide selectivity were calculated to evaluate the catalytic performance of different catalysts and the adsorption performance of the sorbents. They can be defined by the following equations (Eqs. (4)–(7)):

$$CH_4\ \ conversion(\%) = \frac{F_{CH_{4,in}} - F_{CH_{4,out}}}{F_{CH_{4,in}}} \times 100\% \tag{4}$$

$$H_2\ \ yield(\%) = \frac{F_{H_{2,out}}}{4 \bullet F_{CH_{4,in}}} \times 100\% \tag{5}$$

$$H_2\ \ purity(\%) = \frac{F_{H_{2,out}}}{F_{H_{2,out}} + F_{CO_{out}} + F_{CO_{2,out}} + F_{CH_{4,out}}} \times 100\% \tag{6}$$

$$CO\ \ selectivity(\%) = \frac{F_{CO_{out}}}{F_{CO_{out}} + F_{CO_{2,out}}} \times 100\% \tag{7}$$

In which $F_{i,in}$ and $F_{i,out}$ $\left(i = CH_4,\ H_2,\ CO_2,\ CO\right)$ represent the molar flow rate of gas species i in the inlet and outlet streams.

Table 2
Structural characters of different monolith samples.

Technique	Samples	SiC-M	SiC-M-old	SiC-M-40C-old	SiC-M-20PMMA-old
MIP	Porosity (%)	78.4	64.3	68.5	74.4
	Open pore surface area (m^2/g)	5.83	0.13	0.12	0.14
	Average pore diameter (nm)	764	26,823	33,064	37,347
	Permeability (mDa)	183.4	7839	3412	674
	Tortuosity	19.25	3.22	4.68	11.65
	Fractal dimension	2.956	2.960	2.970	2.978
N_2 sorption	BET surface area (m^2/g)	11.26	1.15	2.54	2.60

3. Results and discussion

3.1. Characterisation of monoliths

3.1.1. Porosimetry of different monoliths

Table 2 compares the structural characters of SiC-M–old, SiC-M-40C-old, SiC-M-20PMMA-old, SiC-M monolithic supports. Assuming the contour for the pore and channel were uniform [27], the surface area of open pores was estimated using the formula proposed by Hillar and Carl [28] (Eq. (8)):

$$S = \frac{1}{\sigma M cos(\theta)} \int_0^{V_{max}} PdV \tag{8}$$

In which σ is the surface free energy of liquid mercury in vacuum, M is the sample mass, θ is the contact angle, P is the intrusion pressure, and V is the intrusion volume.

All SiC-M supports exhibited highly porous structures, as their porosities varied from 64.3 to 78.4 %. They exhibit similar and high values of fractal dimensions, which was as expected as the roughness and pore irregularity of these samples were high [27]. However, the different thermal treatments caused a significant structural deformation in terms of pore characteristics and connectivity between the pores, as the surface area, the average pore diameter, the permeability and the tortuosity of SiC-M were significantly different from the 'old batches' samples. When the same sintering process was applied, the average pore diameter increased under different conditions (freezing temperature or second additive), and the open pore surface area slightly changed. In fact, fast freezing can be achieved and smaller ice templates were created when the freezing temperature was lower [29]. These smaller ice templates were more in number and closer to each other, which made it easy to merge. The PMMA particles became the second sacrificial templates that were even bigger than ice templates, and fewer pores were formed. However, the observation of bigger pores seems to contradict the permeability and tortuosity data, as low permeability and high tortuosity were observed which may result in a high pressure drop of the catalysts. These can be explained by the fact that some pores were not open, as MIP doesn't count the closed pores that are not accessible for mercury [30]. There might be some pores that were opened by mercury under pressure during the measurement, which is one of the limitations of MIP.

3.1.2. Specific BET surface area of monoliths

As shown in Table 2, the specific BET surface areas (m^2/g) of different SiC-M monoliths (SiC-M-old, SiC-M-40C-old, SiC-M-20PMMA-old, SiC-M) were compared. Similar results were found, as new batch monoliths (SiC-M) exhibited the highest surface area of 11.26 m^2/g. However, the surface area measured with nitrogen adsorption was much higher than the open pore surface area calculated from MIP data. As N_2 molecules are much more accessible to the smaller pores than mercury, the different surface areas obtained by the N_2 sorption and MIP reveal the existence of the mesopores and micropores for all monolithic samples [31].

3.1.3. Morphology of monoliths

Fig. 2 (a), (b) and (c) show the SEM images of SiC-M-old, SiC-M-40C-old and SiC-M-20PMMA-old. No apparent texture change was found for

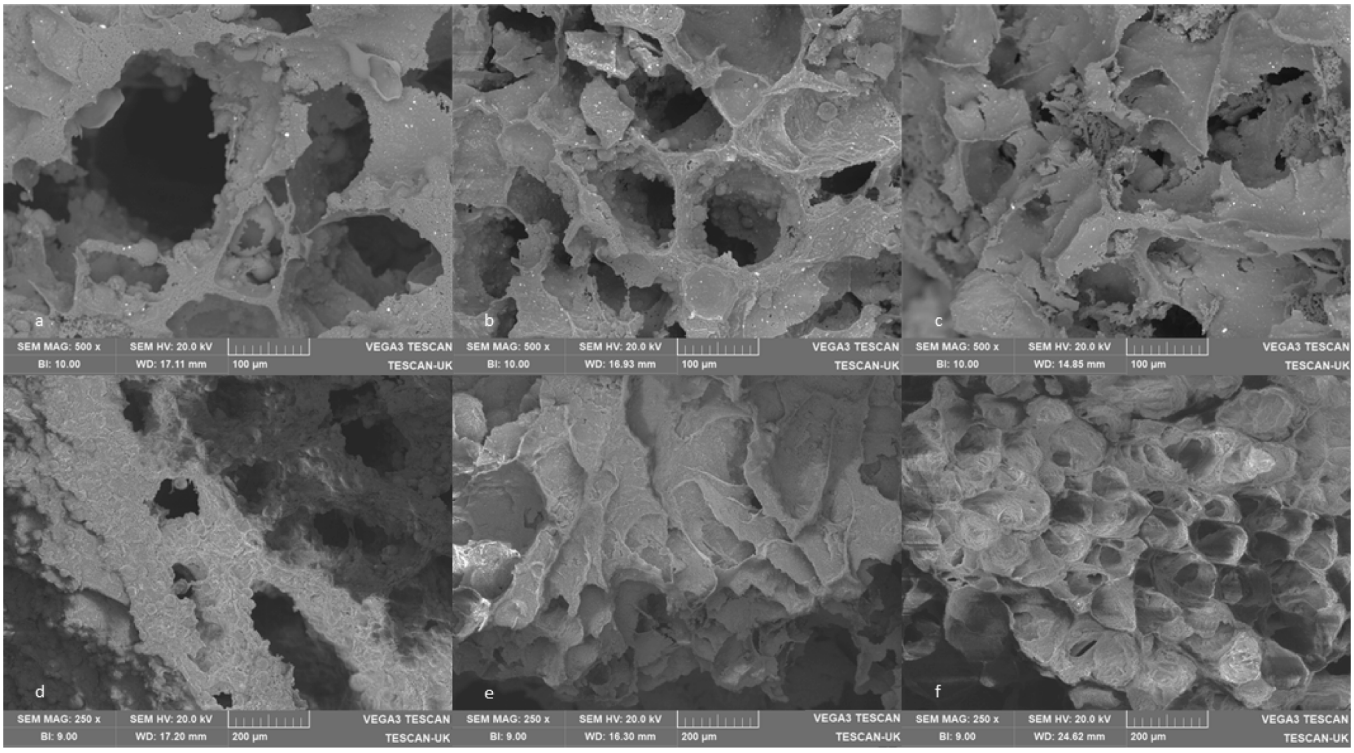

Fig. 2. SEM images of (a) SiC-M-old, (b) SiC-M-40C-old, (c) SiC-M-20PMMA-old, (d) SiC-M, (e) SiC-M-40C, and (f) SiC-M-70C.

Table 3
Metal loading of different monolithic samples.

Monoliths	Nickel loading (in g on NiO)	Nickel loading (in wt.% on NiO)
SiC-M	0.40 ± 0.02	19.3 ± 0.7
SiC-M-40C	0.43	19.7
SiC-M-70C	0.49	22.6
SiC-M-10PMMA	0.36	16.6
SiC-M-20PMMA	0.52	24.4

all samples, revealing that fast freezing and the second pore former have no effect on the material. Regarding the structural outlook, as expected, the pores were smaller when the freezing temperature became lower (Fig. 2 (a) and (b)), confirming the presence of smaller ice templates at that condition. The addition of PMMA templates was found to change the pore shape, as these pores became flatter. Unlike other study [32], the co-worked templates (ice and PMMA) have a negative effect on pore formation. This observation may explain the inconformity of pore diameter data from MIP as the pore diameters cannot be determined accurately when the sphericity is very low.

Fig. 2 (d), (e) and (f) focus on the morphology of SiC-M and the fast-frozen samples (SiC-M-40C and SiC-M-70C). It can be observed that both monoliths under lower freezing temperatures showed a similar appearance, and pores became smaller and shallower compared with the samples prepared at standard conditions (SiC-M). This confirmed the positive effect of freezing temperature over the size of ice templates as pore formers. Also, the shape of the pores can influence the calculated results on pore size using MIP, as these non-spherical pores were

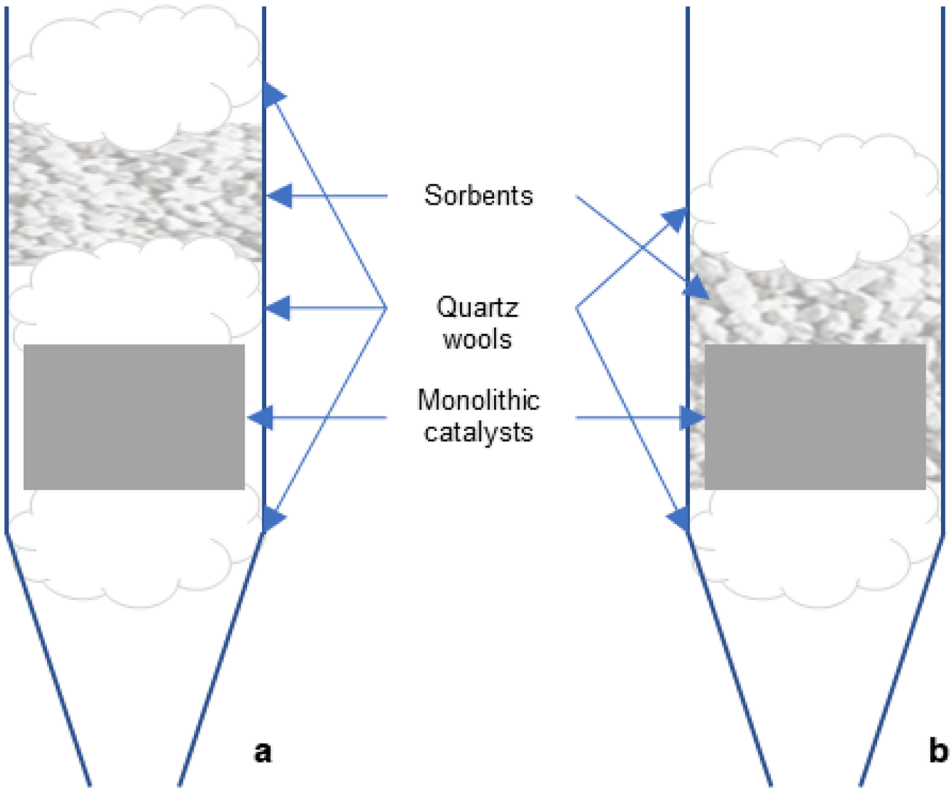

Fig. 3. Topographical illustration of different designs in reactor setup: (a) Design 1 – independent sorbent layer, (b) Design 2 – mixing sorbent.

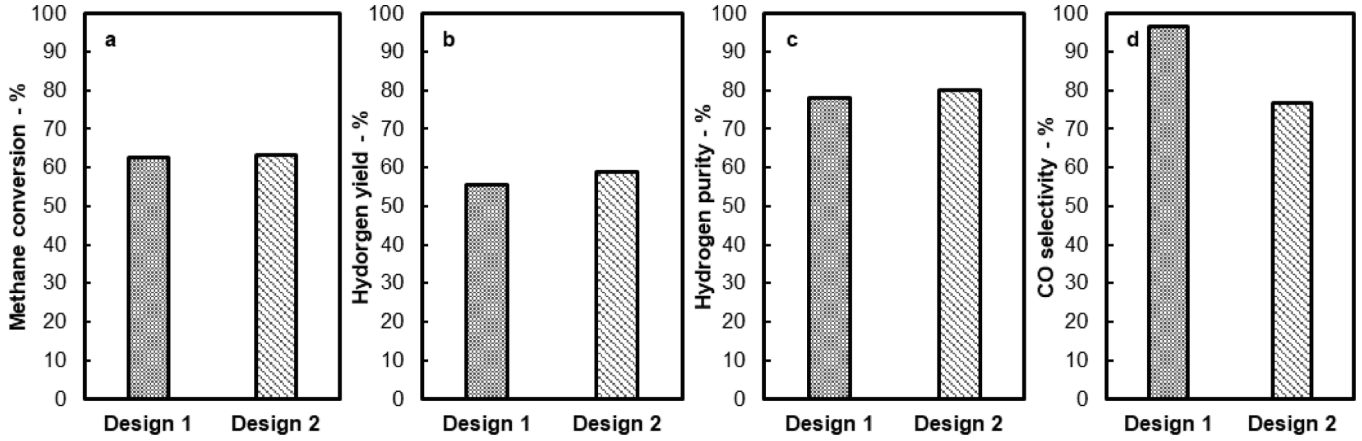

Fig. 4. Catalytic performance of 20Ni/SiC-M catalysts with sorbents (315–400 μm) at 600 °C, S:C = 3, GHSV = 10,000 h^{-1} (a) methane conversion, (b) hydrogen yield, (c) hydrogen selectivity, and (d) CO selectivity.

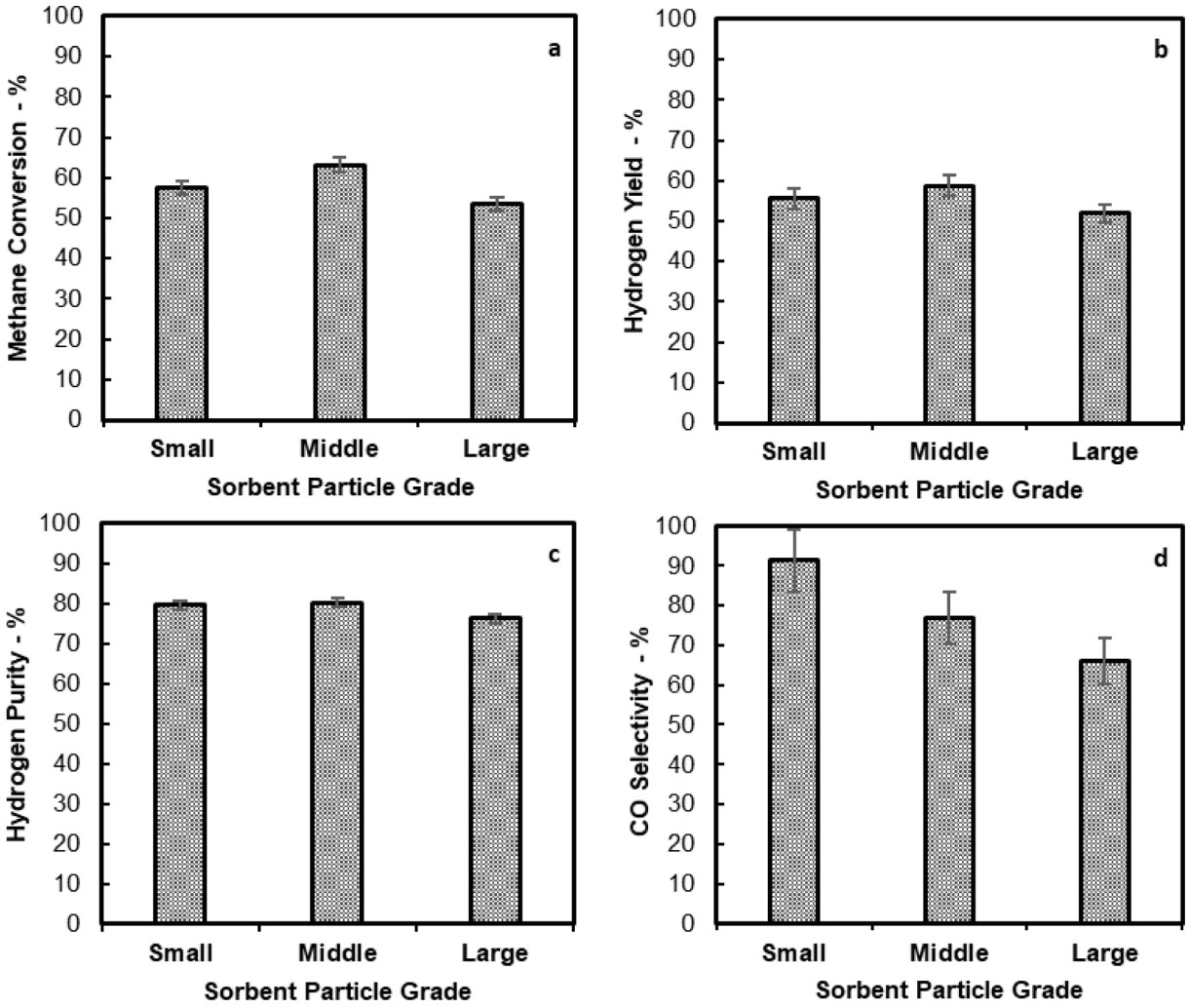

Fig. 5. Catalytic performances of 20Ni/SiC-M catalysts with different grades of calcium sorbents at 600 °C, S:C = 3, 10,000 h^{-1} GHSV, (a) methane conversion, (b) hydrogen yield, (c) hydrogen selectivity, and (d) CO selectivity.

apparently opened in a different direction. In a word, SiC-M-40C and SiC-M-70C were expected to have similar characteristics, whereas the characteristics of SiC-M were different. When Fig. 2 (a) and (d) were compared, it is unlikely to demonstrate any significant effect of sintering conditions over the size of the pores, but as stated in our previous work [19], the morphology of SiC-M was rough and coarse, leading to a significant increase in terms of surface area.

3.1.4. Nickel loading

The actual metal loading on different monoliths (SiC-M, SiC-M-40C, SiC-M-70C, SiC-M-10PMMA, and SiC-M-20PMMA) were evaluated and shown in Table 3. For SiC-M, three measurements were conducted using samples from different batches to evaluate the standard deviation of nickel loading.

It can be observed that the actual nickel loading of 20Ni/SiC-M was about 0.4 g in NiO. The structure of monoliths has a limited effect when the same ice template is applied, as they have similar surface characteristics. However, the PMMA template seems to impose uncertainty on metal loading, as the loading varied beyond the error coming from the wet impregnation technique.

3.2. Catalytic performance

3.2.1. Primary tests

Two designs were tested in the primary tests: one was to add an independent layer of sorbents on the top of the monolith, separated by a thin layer of quartz wool; another was to mix the sorbents from the top of the monolith, in this case, sorbents and catalyst were contacted (illustrated in Fig. 3).

The GHSV value was calculated using the total volume of monolithic catalysts and sorbents, assuming that they were incompressible. For these two designs, the former required a higher total gas flow as the volume of quartz wool between monolith and sorbent was considered in the GHSV estimation. When the gas was switched to the gas mixture of methane/nitrogen, the SMR reaction occurred within tens of seconds to reach the breakthrough point. Data were then collected during the steady state of the reaction. Fig. 4 compares the two designs (Design 1: independent sorbent layer, Design 2: mixing sorbent) in terms of methane conversion, hydrogen yield, hydrogen purity, and carbon monoxide selectivity.

It can be clearly observed that the catalytic performance using the two designs was similar, in terms of methane conversion, hydrogen yield, and hydrogen purity. At 600 °C, 1 bar, steam to carbon ratio of 3, and with a GHSV value of 10,000 h^{-1}, methane conversion reached 62–63 %, hydrogen yield reached 55–57 %, and hydrogen purity was around 80 %. However, these values were smaller than that for the SMR test using the same catalysts, which was reported in our previous work [19]. This can be explained by the dilution effect caused by the increase of total gas flow to maintain the same gas space velocity. As the limestone particles were loose, the apparent volumetric density of sorbent

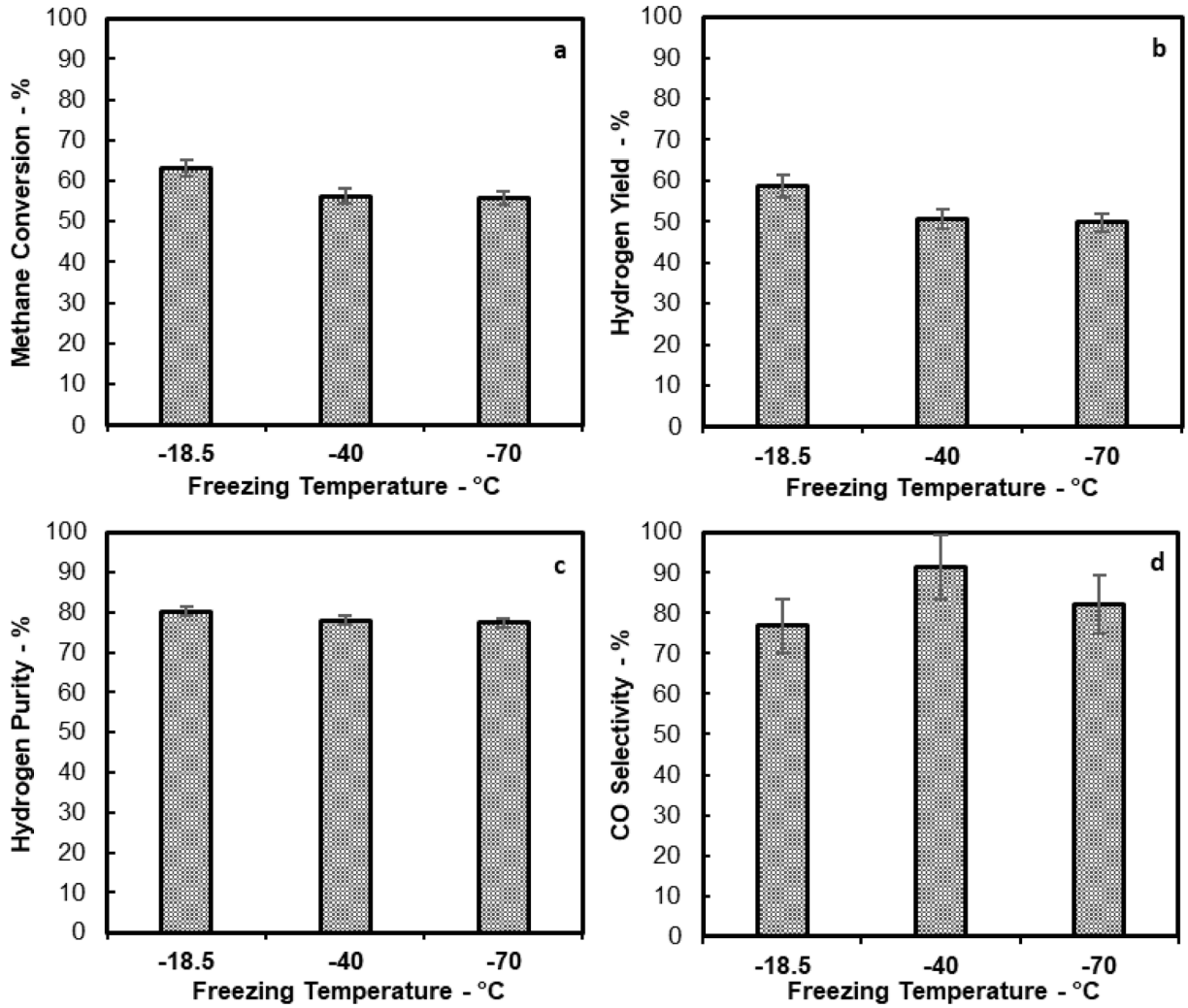

Fig. 6. Catalytic performances of 20Ni/SiC-M, 20Ni/SiC-M-40C, and 20Ni/SiC-M-70C catalysts with middle grade (315–400 μm) of calcium sorbents at 600 °C, S:C = 3, 10,000 h^{-1} GHSV, (a) methane conversion, (b) hydrogen yield, (c) hydrogen selectivity, and (d) CO selectivity.

was greater than the material, which is 2.65. Herein, the height of the sorbent layer was measured, which was about 8–10 mm, and the volume of the sorbent layer was similar to that of the monolithic catalysts. The catalysts showed similar activities, whether sorbents were added or not.

When the sorbents were added, the carbon monoxide selectivity was much higher than the results for catalyst only found in our previous study for both designs (97 % vs 55 %, 77 % vs 55 %, respectively) [19], indicating that carbon dioxide was adsorbed by the sorbent efficiently. When the sorbents were separated from the monolithic catalyst (Design 1), a better carbon monoxide selectivity was found, meaning that a higher CO_2 capture efficiency was achieved by the independent sorbent layer.

The following experiments were conducted using one of the designs: the sorbents were mixed with the monolithic catalysts without physical separation (Design 2). This design was selected as it minimised the errors from the additional quartz wool layer that may cause a slight decrease in catalytic performances.

3.2.2. *Effect of sorbent particle size*

The catalytic performance of 20Ni/SiC-M with three grades of sorbents (small: 200–315 μm, middle: 315–400 μm, large: 400–500 μm) was shown in Fig. 5, in terms of methane conversion, hydrogen yield, hydrogen purity, and carbon monoxide selectivity. All tests were performed at 600 °C, steam to carbon ratio of 3, 1 bar, and GHSV of 10,000 h^{-1}. 20Ni/SiC-M and middle grade sorbent (315–400 μm) were chosen to evaluate the standard deviation of the SE-SMR system by three repetitions using different batches of catalysts and sorbents. The standard deviation data were applied for all tests that followed.

It can be observed that methane conversion and hydrogen yield achieved the highest values with the middle grade limestones (315–400 μm), which were 63 % and 59 %, respectively. Hydrogen purity was maintained at around 80 % for all the ranges of limestones studied. These performance data were close to the results reported by García-Lario et al., which were also not far from the equilibrium data they calculated [33]. CO selectivity decreased when the particle size of the sorbent increased from 91 % to 66 %. The CO selectivity reduced as less CO_2 gas was adsorbed by limestones, and as reported by Santiago et al., the CO_2 sorption rate increased when the particle size of sorbents was decreased [34]. This is because the large particles suffer from high mass transfer limitations [35], resulting in the reduction of catalyst activities. However, the decrease in catalytic activities when small particles were applied seems to contradict the previous statement. When small grade limestones were used, the pressure drops were high, but the adsorbent activities should not be restricted. The possible reason could be the non-conformity of sorbent particle size and pore size of monolithic catalysts, which were 200–315 μm and 70–140 μm [19], respectively. The available pores within the catalysts were partially blocked by the sorbent particles, leading to lower catalytic activity. During the tests, the bigger sorbent particles sat on the smaller open pores/channels and impeded the mass transportation to the active sites inside the pores. In

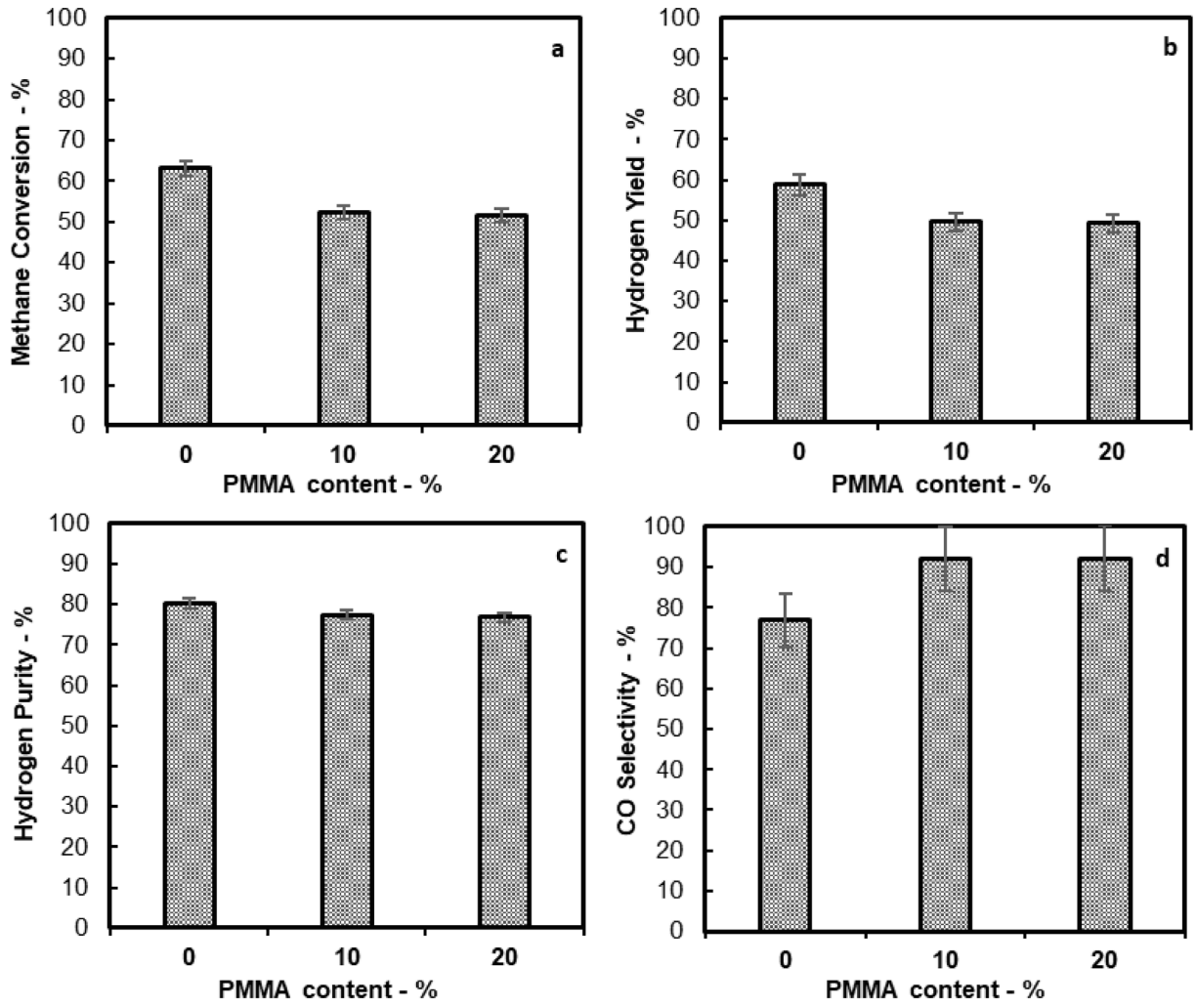

Fig. 7. Catalytic performances of 20Ni/SiC-M, 20Ni/SiC-M-10PMMA and 20Ni/SiC-M-20PMMA catalysts with middle grade (315–400 μm) of calcium sorbents at 600 °C, S:C = 3, 10,000 h^{-1} GHSV, (a) methane conversion, (b) hydrogen yield, (c) hydrogen selectivity, and (d) CO selectivity.

conclusion, the combination of the middle grade (315–400 μm) limestones with 20Ni/SiC-M catalysts was found to be optimal.

3.2.3. *Effect of freezing temperature*

Fig. 6 shows the results of experiments using different monolithic catalysts (20Ni/SiC-M, 20Ni/SiC-M-40C, and 20Ni/SiC-M-70C) and the middle range of sorbents (315–400 μm), in terms of methane conversion vs freezing temperature, hydrogen yield vs freezing temperature, hydrogen selectivity vs freezing temperature, and CO selectivity vs freezing temperature.

The results highlight the negative effect of smaller pore formers on catalytic activities under SE-SMR conditions. Both methane conversion and hydrogen yield reduced when the freezing temperature decreased, but the difference between 20Ni/SiC-M-40C and 20Ni/SiC-M-70C was insignificant. As mentioned in Section 3.1.1, the smaller pores formed under lower freezing temperatures increase the permeability and tortuosity of the structure. Assuming the distribution of the active metal was identical for all samples, gas species were unlikely to be chemisorbed on the surface of pores due to the high pressure drops. The similar morphology of SiC-M-40C and SiC-M-70C monoliths (See Section 3.1.3) explains their similar catalytic performance and also supports the strong structural effect on surface reactions. Similar average pore size and pore numbers were reported by Fukushima et al. when the freezing temperature was below −40 °C [22]. Hydrogen purity and CO selectivity of 20Ni/SiC-M-40C and 20Ni/SiC-M-70C were not significantly changed, compared with 20Ni/SiC-M. It suggests that the catalytic activity of structured catalysts depends mainly on the characteristics of hydrodynamic flow features (e.g. pressure drops).

3.2.4. *Effect of PMMA ratio*

The performance of 20Ni/SiC-M, 20Ni/SiC-M-10PMMA and 20Ni/SiC-M-20PMMA combined with limestones in a range of 315–400 μm under SE-SMR conditions (600 °C, 1 bar, S:C = 3, GHSV = 10,000 h^{-1}) was shown in Fig. 7, in terms of methane conversion vs PMMA content, hydrogen yield vs PMMA content, hydrogen selectivity vs PMMA content, and CO selectivity vs PMMA content.

The catalytic activity was not improved by adding PMMA templates, as methane conversion and hydrogen yield were decreased. When PMMA was added, the permeability of the monolith decreased significantly, and the tortuosity increased (See Section 3.1.1), as a result, the pressure drops at the catalyst were higher than the samples without PMMA. This could be the key factor to influence catalysts' performance. However, hydrogen purity was slightly reduced, and CO selectivity was obviously increased, for both samples with PMMA. Less methane was converted, and less hydrogen was produced, resulting in a lower hydrogen purity; less CO and CO_2 were produced, leading to a higher CO selectivity when CO_2 was rapidly adsorbed. It seems that the pore shape had limited effects on catalytic activity, whereas the flow did. The similar performance between the 20Ni/SiC-M-10PMMA and 20Ni/SiC-M-20PMMA indicates that they had similar structural properties (e.g.

permeability, tortuosity) and morphology, and PMMA templates worked in a negative way with ice templates. The size of the templates, not the amount, was the key feature to modify the structure.

4. Conclusions

Monolithic nickel-based catalysts with various pore characters were tested under typical SE-SMR conditions (600 °C, 1 bar, S:C = 3) and high gas space velocity (10,000 h^{-1}), coupled with different grades of limestones as sorbents. The results demonstrated that the catalytic performance of structured catalysts had a strong relationship with the pressure drops, that was controlled by pores and channels, ignoring the shape and amount. It indicated that the limitations of the internal mass diffusion of gas compounds were also important. For monolithic Ni/SiC-M catalysts, sorbents were proven to adsorb CO_2 gases efficiently in a dynamic flow, and small pores were not favourable for improving the activities. The limitations of this study include the following: (1) the recycling of sorbents was not considered, as sorbents were renewed each time with fresh samples; (2) a low pressure drop structure was not constructed due to the lack of equipment, but it would be of interest to validate the results using an appropriate freezing temperature (e.g. −5 °C) for preparation; (3) the stability of the catalyst was not evaluated, as all results were obtained in the pre-breakthrough stage of the sorbents, and the duration of each experiment was limited by the amount of sorbents.

Funding

This research did not receive any specific grant from funding agencies in the public, commercial, or not-for-profit sectors.

CRediT authorship contribution statement

Ziqi Shen: Writing – original draft, Visualization, Methodology, Investigation, Formal analysis, Conceptualization. **Seyed A. Nabavi:** Writing – review & editing, Supervision, Methodology, Conceptualization. **Peter T. Clough:** Writing – review & editing, Supervision, Project administration, Methodology, Conceptualization.

Declaration of competing interest

The authors declare that they have no known competing financial interests or personal relationships that could have appeared to influence the work reported in this paper.

Acknowledgements

The authors wish to thankfully acknowledge Dr David Danaci and Dr Jose Juan Morales Corona for their help in performing MIP characterisation. The authors would also like to thank Dr Siqi Wang for her help proofreading the manuscript. For the purposes of open access, the author has applied a Creative Commons Attribution (CC BY) licence to any Accepted Author Manuscript version arising from this submission.

References

[1] United Nations Environment Programme & IP on CC. Climate Change 2007: The Physical Science Basis; Contribution of Working Group I to the Fourth Assessment Report of the Intergovernmental Panel on Climate Change - Summary for Policymakers. 2007.
[2] Caroline Pereira Oliveira A, Bruno Lima Santos D, Gomes Moura L, Eponina HC. Sorption-enhanced steam reforming of propane using bifunctional Ni/CaO, Ni/CaO-CaZrO3, and Ni/CaO-Ca2SiO4 catalysts. Fuel 2024:358. https://doi.org/10.1016/j.fuel.2023.130170.
[3] Welsby D, Price J, Pye S, Ekins P. Unextractable fossil fuels in a 1.5 °C world. Nature 2021;597:230–4. https://doi.org/10.1038/s41586-021-03821-8.
[4] EU's Copernicus Climate Change Service. Global temperature trend monitor n.d. https://cds.climate.copernicus.eu/cdsapp#!/software/app-c3s-global-temperature-trend-monitor?tab=app (accessed May 7, 2024).
[5] International Energy Agency. Global Hydrogen Review 2022. 2022.
[6] Wang S, Nabavi SA, Clough PT. A review on bi/polymetallic catalysts for steam methane reforming. Int J Hydrogen Energy 2023. https://doi.org/10.1016/j.ijhydene.2023.01.034.
[7] Ahn SY, Kim KJ, Kim BJ, Hong GR, Jang WJ, Bae JW, et al. From gray to blue hydrogen: Trends and forecasts of catalysts and sorbents for unit process. Renew Sustain Energy Rev 2023:186. https://doi.org/10.1016/j.rser.2023.113635.
[8] Li T, Tsubaki N, Jin Z. S-scheme heterojunction in photocatalytic hydrogen production. J Mater Sci Technol 2024;169:82–104. https://doi.org/10.1016/J.JMST.2023.04.049.
[9] Yang C, Li X, Li M, Liang G, Jin Z. Anchoring oxidation co-catalyst over CuMn2O4/graphdiyne S-scheme heterojunction to promote eosin-sensitized photocatalytic hydrogen evolution. Chin J Catal 2024;56:88–103. https://doi.org/10.1016/S1872-2067(23)64563-2.
[10] IEA. IEAGHG Technical Review Reference data and Supporting Literature Reviews for SMR Based Hydrogen Production with CCS. 2017.
[11] Dou B, Wang C, Song Y, Chen H, Jiang B, Yang M, et al. Solid sorbents for in-situ CO2 removal during sorption-enhanced steam reforming process: A review. Renew Sustain Energy Rev 2016;53:536–46. https://doi.org/10.1016/j.rser.2015.08.068.
[12] Kierzkowska AM, Pacciani R, Müller CR. CaO-based CO2 sorbents: From fundamentals to the development of new, highly effective materials. ChemSusChem 2013;6:1130–48. https://doi.org/10.1002/CSSC.201300178.
[13] Bhatia SK, Perlmutter DD. Effect of the product layer on the kinetics of the CO2-lime reaction. AIChE J 1983;29:79–86. https://doi.org/10.1002/AIC.690290111.
[14] Seman MHA, Othman NH, Osman N, Jani AMM. Nickel based catalysts supported on porous support for methane steam reforming: potential and short review. In: IOP Conf Ser Earth Environ Sci, vol. 1151. Institute of Physics; 2023. https://doi.org/10.1088/1755-1315/1151/1/012061.
[15] Nieva MA, Villaverde MM, Monzón A, Garetto TF, Marchi AJ. Steam-methane reforming at low temperature on nickel-based catalysts. Chem Eng J 2014;235:158–66. https://doi.org/10.1016/J.CEJ.2013.09.030.
[16] Obradović A, Likozar B, Levec J. Catalytic surface development of novel nickel plate catalyst with combined thermally annealed platinum and alumina coatings for steam methane reforming. Int J Hydrogen Energy 2013;38:1419–29. https://doi.org/10.1016/J.IJHYDENE.2012.11.015.
[17] Obradović A, Likozar B, Levec J. Steam methane reforming over Ni-based pellet-type and Pt/Ni/Al 2O3 structured plate-type catalyst: Intrinsic kinetics study. Ind Eng Chem Res 2013;52:13597–606. https://doi.org/10.1021/IE401551M/ASSET/IMAGES/LARGE/IE-2013-01551M_0011.JPEG.
[18] Lorber K, Zavašnik J, Arčon I, Huš M, Teržan J, Likozar B, et al. CO2Activation over Nanoshaped CeO2Decorated with Nickel for Low-Temperature Methane Dry Reforming. ACS Appl Mater Interfaces 2022;14:31862–78. https://doi.org/10.1021/ACSAMI.2C05221/ASSET/IMAGES/LARGE/AM2C05221_0010.JPEG.
[19] Shen Z, Nabavi SA, Clough PT. Design and performance testing of a monolithic nickel-based SiC catalyst for steam methane reforming. Appl Catal A Gen 2024;670:119529. https://doi.org/10.1016/j.apcata.2023.119529.
[20] Karadeniz H, Karakaya C, Tischer S, Deutschmann O. Numerical simulation of methane and propane reforming over a porous Rh/Al2O3 catalyst in stagnation-flows: Impact of internal and external mass transfer limitations on species profiles. Catalysts 2020;10:1–25. https://doi.org/10.3390/catal10080915.
[21] Eom J-H, Kim Y-W, Raju S. Processing and properties of macroporous silicon carbide ceramics: A review. J Asian Ceram Soc 2013:1. https://doi.org/10.1016/j.jascer.2013.07.003.
[22] Fukushima M, Nakata M, Zhou Y, Ohji T, Yoshizawa Y. Fabrication and properties of ultra highly porous silicon carbide by the gelation-freezing method. J Eur Ceram Soc 2010;30:2889–96. https://doi.org/10.1016/j.jeurceramsoc.2010.03.018.
[23] Hotza D, Di Luccio M, Wilhelm M, Iwamoto Y, Bernard S, Diniz da Costa JC. Silicon carbide filters and porous membranes: A review of processing, properties, performance and application. J Memb Sci 2020:610. https://doi.org/10.1016/j.memsci.2020.118193.
[24] Li X, Li Y, Guo X, Jin Z. Design and synthesis of ZnCo2O4/CdS for substantially improved photocatalytic hydrogen production. Front Chem Sci Eng 2023;17:606–16. https://doi.org/10.1007/S11705-022-2233-4/METRICS.
[25] Theo Stein. Carbon dioxide now more than 50% higher than pre-industrial levels. National Oceanic and Atmospheric Administration 2022. https://www.noaa.gov/news-release/carbon-dioxide-now-more-than-50-higher-than-pre-industrial-levels (accessed December 29, 2023).
[26] Gravogl G, Birkelbach F, Müller D, Lengauer CL, Weinberger P, Miletich R. Pressure dependence of the low temperature carbonation kinetics of calcium oxide for potential thermochemical energy storage purposes and sustainable CO2 fixation. Adv Sustain Syst 2021:5. https://doi.org/10.1002/adsu.202100022.
[27] Li W, Chen ZH. Characterization of partially densified 3D Cf/SiC composites by using mercury intrusion porosimetry and nitrogen sorption. Ceram Int 2008;34:531–5. https://doi.org/10.1016/j.ceramint.2006.11.015.
[28] Hillar MR, Carl FP. Surface areas from mercury porosimeter measurements. J Phys Chem 1967;71:2733–6.
[29] Hsieh CY, Tsai SP, Ho MH, Wang DM, Liu CE, Hsieh CH, et al. Analysis of freeze-gelation and cross-linking processes for preparing porous chitosan scaffolds. Carbohydr Polym 2007;67:124–32. https://doi.org/10.1016/j.carbpol.2006.05.002.
[30] Plötze M, Niemz P, Plötze M, Plötze M, Zurich E, Niemz P. Porosity and pore size distribution of different wood types as determined by mercury intrusion porosimetry. Eur J Wood Wood Prod 2011;69:649–57. https://doi.org/10.3929/ethz-b-000039735.
[31] Hellmuth K-H, Klobes P, Meyer K, Röhl-Kuhn B, Siitari-Kauppi M, Hartikainen J, et al. Matrix retardation studies: Size and structure of the accessible pore space in fresh and altered crystalline rock. Geowissenschaften Wutzke 1995:691–706.

[32] Song IH, Kwon IM, Kim HD, Kim YW. Processing of microcellular silicon carbide ceramics with a duplex pore structure. J Eur Ceram Soc 2010;30:2671–6. https://doi.org/10.1016/j.jeurceramsoc.2010.04.027.
[33] García-Lario AL, Grasa GS, Murillo R. Performance of a combined CaO-based sorbent and catalyst on H2 production, via sorption enhanced methane steam reforming. Chem Eng J 2015;264:697–705. https://doi.org/10.1016/j.cej.2014.11.116.
[34] Santiago R, Lemus J, Hospital-Benito D, Moya C, Bedia J, Alonso-Morales N, et al. CO2 capture by supported ionic liquid phase: Highlighting the role of the particle size. ACS Sustain Chem Eng 2019;7:13089–97. https://doi.org/10.1021/acssuschemeng.9b02277.
[35] Xie M, Zhou Z, Qi Y, Cheng Z, Yuan W. Sorption-enhanced steam methane reforming by in situ CO 2 capture on a CaO-Ca 9Al 6O 18 sorbent. Chem Eng J 2012;207–208:142–50. https://doi.org/10.1016/j.cej.2012.06.032.